Article

Detection of Extreme Phenomena in the Stable Boundary Layer over the Amazonian Forest

Francisco O. Miranda [1,2,*,†], **Fernando M. Ramos** [3], **Celso von Randow** [3],
Cléo Q. Dias-Júnior [2,4], **Marcelo Chamecki** [5], **Jose D. Fuentes** [6], **Antônio O. Manzi** [2,7] **and**
Marceliano E. de Oliveira [1] **and Cledenilson M. de Souza** [8]

1   UEA/CESP—Amazonas State University, Parintins 69153-230, Amazonas, Brazil; meoliveira@uea.edu.br
2   INPA/CLIAMB—National Institute of Amazon Researches, Manaus 69060-001, Amazonas, Brazil;
     cleo.quaresma@ifpa.edu.br (C.Q.D.-J.); antonio.manzi@inpe.br (A.O.M.)
3   CCST/INPE—National Institute for Space Research, São José dos Campos, São Paulo 12630-000, Brazil;
     fernando.ramos@inpe.br (F.M.R.); celso.vonrandow@inpe.br (C.v.R.)
4   IFPA—Federal Institute of Education Science and Tecnology, Belém, Pará 36180-000, Brazil
5   Department of Atmospheric and Oceanic Sciences, University of California, Los Angeles, CA 90095, USA;
     chamecki@ucla.edu
6   Department of Meteorology and Atmospheric Science, The Pennsylvania State University,
     University Park, PA 16801, USA; juf15@psu.edu
7   CPTEC/INPE—National Institute for Space Research, São José dos Campos, São Paulo 12630-000, Brazil
8   UFAM—Federal University of Amazonas, Parintins 69067-005, Amazonas, Brazil;
     cledenilsonms@ufam.edu.br
*   Correspondence: ffarias@uea.edu.br
†   Current address: Department of Physics, Amazonas State University (CESP/UEA), Parintins 69067-005,
     Amazonas, Brazil.

check for updates

Abstract: We apply different methods for detection of extreme phenomena (EP) in air-turbulent time series measured in the nocturnal boundary layer above the Amazon forest. The methods used were: (a) a Morlet complex wavelet transform, which is often used in analysis of non-linear application processes. Through the use of the wavelet, it is possible to observe a phase singularity that involves a strong interaction between an extensive range of scales; (b) recurrence plot tests, which were used to identify a sudden change between different stable atmospheric states. (c) statistical analysis of early-warning signals, which verify simultaneous increases in the autocorrelation function and in the variance in the state variable; and (d) analysis of wind speed versus turbulent kinetic energy to identify different turbulent regimes in the stable boundary layer. We found it is adequate to use a threshold to classify the cases of strong turbulence regime, as a result of the occurrence of EP in the tropical atmosphere. All methods used corroborate and indicate synergy between events that culminate in what we classify as EP of the stable boundary layer above the tropical forest.

Keywords: extreme phenomena; turbulence regimes; nocturnal boundary layer

1. Introduction

Many of the techniques used for the analysis of micrometeorological data do not take into account situations where extreme phenomena (EP) are manifested. Here, EP are defined as sudden variations that occur simultaneously in several time series of thermodynamic and chemical species variables, measured at the forest-atmosphere interface. It is known that the manifestation of these phenomena in the Amazonian nocturnal boundary layer (NBL) is generally associated with strong turbulent exchange between vegetation and the atmosphere [1–5]. The detection and prediction of EP in geophysics,

ecology, economy and other knowledge fields have already received attention [6–10], although these EP have different natures. The occurrence of an EP might be characterized as an emergent phenomenon in non-linear processes as discussed in a general way by [11–13] and in specific applications by [14–16], among others. Such processes are often associated with the emergence of critical slowing down, where a system is close to a critical tipping point and recovery rates of equilibrium states decrease, which have been observed in distinct scientific domains. Weng and Lau, and Lau and Weng [17,18] studied the occurrence of EP in the tropical atmosphere of Indonesia. They observed that during the outbreak of the EP, phase singularities (that involves a strong interaction between an extensive range of scales) appear in diagrams produced with Morlet's wavelet transform.

The recurrence plot (RP) technique is also useful to identify the occurrence of EP [19,20]. According to [20] the occurrence of these phenomena is always associated with sudden changes in the dynamics of the system, producing two qualitatively distinct states. They noticed changes on the texture patterns of the recurrence plot during the appearance of an EP. Trulla et al. [19] also verified the appearance of recurrence points (marked with darker colors in the RP) with the proximity of an EP. In addition to the aspects mentioned above, some studies reveal that the occurrence of such phenomena in the stable boundary layer are likely related to a transition that marks a change in turbulent regimes [21], or beyond transitions between regimes as verified by [22–24]. These authors mention the transition from weak to strong turbulence thresholds (referred here as λ_1). However, some recent results have revealed the need to define a second mode of transition threshold between nocturnal turbulence regimes (λ_2), associated with a threshold of transition between a regime of strong turbulence (regime 2 according to the classification of [25]) to another regime called here "very strong turbulence". Values greater than λ_2 can be observed in the SBL during the presence of convective clouds and strong downdrafts above the Amazon rainforest [3,26,27]. The complexity of the biosphere-atmosphere interaction processes are amplified by the presence of external forcing, such as convective clouds [26]. It is known that during the top-down movement of air parcels arising from higher levels of the atmosphere, which are colder and drier, going into the forest canopy, hotter air (and other particles inside the forest canopy) are being ejected from the forest canopy into the lower layers of the atmosphere.

The possibility of the existence of a second transition threshold was also reported by [28] in their analysis of the variability of carbon dioxide concentration statistics in relation to the average wind speed for the tropical forest region. Acevedo et al. [29], using data from experimental sites located in mid-latitudes, show that for situations of very strong turbulence regime there is an atmospheric condition in which they call "fully coupled state". Farias [21] reported that a very strong turbulence regime was associated with the occurrence of an EP. The association between EP warning conditions and turbulence regime changes might be used to improve turbulence mixing parameterizations in numerical models to better quantify the fluxes as well as the chemistry of reactive gases in the NBL, among other environmental indicators [4,30,31].

This work intends to show that during the occurrence of an EP in the stable boundary layer over the Amazon forest, it is possible to use different techniques both for the detection and for a better characterization of these phenomena. It should be noted that the occurrence of these phenomena seems to converge to the same condition of variability (to a singular point), such as: (i) the emergence of phase singularities in wavelets analyses, (ii) sudden variations in sensible heat and momentum fluxes near the surface and (iii) changes of the turbulent regimes (transition between the thresholds λ_1 and λ_2).

2. Materials and Methods

2.1. Data

The data used in this work were collected during the rainy seasons of the years 2013 (from January to May) and 2014 (from January to May and December). Data from the dry seasons of the two years

were also analyzed, but events of EP were not detected. The site is located 60 km north of the city of Manaus at Cuieiras reserve ($2° 36.11'$ S–$60° 12.56'$ W, Figure 1), in a typical Amazonian terra firme forest [32]. In this work, five cases of EP occurrence were detected and analyzed, in 2 May 2013; 24 March, 13 April, 16 May and 8 December 2014. However, only the case of 13 April 2014, from 01 to 05 UTC (UTC = local time + 4 h) is presented in the manuscript. For other cases, we performed EWS tests and recurrence plot analysis for wind speed and temperature data. These cases are presented in the supplementary material.
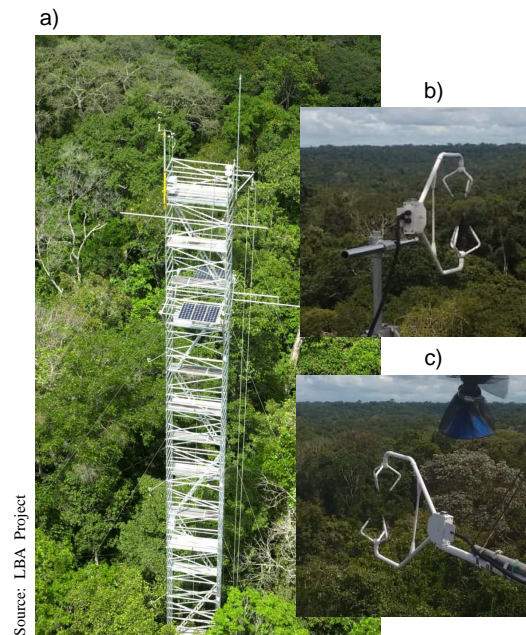
Figure 1. Some characteristics of the experimental site. (**a**) Micrometeorological tower located at Cuieiras reserve. (**b**,**c**) show 3-D sonic anemometer at 48 and 40 m above the ground. Source: http://lba2.inpa.gov.br/index.php/estacoes-de-pesquisa/zf-2-manaus/miss%C3%A3o-hist%C3%B3ria.html.

Time series of horizontal and vertical components of wind velocity (u, v, w), and the sonic virtual air temperature (T_V), measured at 48.15 m above ground with 3-D sonic anemometers (model CSAT3, Campbell Scientific Inc., Logan, UT, USA) at a rate of 20 Hz were used in the analyses. Also, ozone mixing ratio (O_3), humidity and pressure data measured at a height of 35 m were used, with a sampling rate of 1 Hz. To match this, the 3-D sonic anemometer data were later resampled to the sampling frequency of 1 Hz. For cloud cover analyses, available radar images, obtained every 12 min, were used. For more details see [26].

2.2. Methods

The methods used in this work are briefly presented in the following four topics. The first method uses time-frequency diagram of the phases of Morlet's wavelet coefficients, as used by [17]. The second deals with the analysis and classification of turbulence regimes in the tropical atmosphere. The third uses recurrence analysis applied to turbulent signals and was based on the work of [20]. The fourth deals with the early-warning signals and their possible applicability to EP that occur in the tropical atmosphere. Other detailed description of the methods used herein, are provided by [17], explaining the emergence of a phase singularity in a range of various scales during convective processes in the Indonesian atmosphere; by [25] for analyses of turbulence regimes; by [33] explaining the applications and limitations of early-warning signals in dynamic systems; and by [20] for a better understanding of the methods of recurrence analysis applied for complex systems.

2.2.1. Morlet Wavelet Transform

The wavelet transform decomposes a given signal $s(t)$ into elementary functions $\psi_{\beta,\alpha}(t)$ derived from a function called the mother wavelet. This decomposition is carried out by translation and dilatation of the "mother wavelet" and displaced along the time to generate a family of "daughter wavelets", which are expressed as function of two parameters: one for the scales (α), and other for the time position (β) [34,35]:

$$\psi_{\beta,\alpha}(t) = \frac{1}{\sqrt{\alpha}} \psi \left(\frac{t - \beta}{\alpha} \right) \tag{1}$$

where $\alpha, \beta \in \mathbb{R}$, with $\alpha > 0$. A normalization factor $(\alpha)^{-1/2}$ is introduced in Equation (1) to maintain the energy of the mother wavelet across the entire wavelet family used. The wavelet transform of a real signal $s(t)$ is defined in relation to the analysis wavelet $\psi(t)$ as [18]:

$$W(\beta,\alpha) = \frac{1}{\sqrt{\alpha}} \int \psi^* \left(\frac{t - \beta}{\alpha} \right) s(t) dt \tag{2}$$

where ψ^* is the complex conjugate of ψ defined in the "time-scale" real semi-plane (β, α). According to [35] it is possible to obtain the phase $\phi(\beta, \alpha)$ of the signal, in an instant β and on a scale α according to the expression:

$$\phi(\beta,\alpha) = arctan \left(\frac{Im[W(\beta,\alpha)]}{Re[W(\beta,\alpha)]} \right) \tag{3}$$

In this work, Morlet complex wavelet was used, given by:

$$\phi(t) = exp(ik_\psi t) exp \left(\frac{-|t|^2}{2} \right) \tag{4}$$

Among the advantages of using Morlet wavelet, the following stand out: (a) its complex character that facilitates the analysis by scale of the signal phase [17]; (b) the possibility of detecting singularities observing the convergence of continuous phase lines in time-frequency phase spaces (which we will call here phase singularities, as defined by [17]; (c) allows the detection of frequency structure of non-linear dynamic processes containing quasi-periodicity and bifurcations [18].

Similar to the methods used by [17] in their analyzed cases of convective processes in the Indonesian atmosphere, we use Morlet wavelet transform to obtain the time signal phase, to construct an abstract singularity detection space (a phase space), which can be identified by the confluence of lines of the same phase in a time-scale diagram. Furthermore, in that work, several different examples of applications in geophysics are brought up, of what has been called "subharmonic cascade or period doubling route to chaos" in the specialized literature on non-linear dynamics [12] (chapters 13 and 14). By applying this methodology to our experimental data, we were able to characterize the region where there is an occurrence of EP (region where there is a phase singularity).

2.2.2. Turbulence Regimes

Historically, a phase space diagram has been used to classify different turbulence regimes that occur in atmospheric night environments. Such phase space consisted of a diagram proposed by [25], in which a velocity scale associated with turbulent kinetic energy ($V_{TKE} = [1/2(\sigma_u^2 + \sigma_v^2 + \sigma_w^2]^{1/2} = (TKE)^{1/2}$) was plotted on the ordinate axis as a function of the average wind speed ($V_M = (u^2 + v^2)^{1/2}$) measured in the NBL, plotted on the abscissa axis. In this work this diagram was used to assess the threshold values of horizontal wind speed, λ_1 and λ_2, which are associated with the speeds observed during the transitions between the weak to strong turbulence regimes and between the strong to very strong turbulence regimes, respectively. The values of V_{TKE} and V_M in this analysis correspond to averages of 5 min of data [24,36].

To determine λ_1, mean values and standard deviations of V_{TKE} were plotted against each interval of 0.5 m s^{-1} of V_M over the entire available dataset. It was observed that in the region of $V_M = 2.2$ m s^{-1}, an abrupt change in the mean values of V_{TKE} occurred. In this way all situations in which the wind speed was above $\lambda_1 = 2.2$ m s^{-1} but less than λ_2 were associated with strong turbulent regime.

The second transition threshold, λ_2, was determined from a plot of V_M versus kurtosis of the concentration of carbon dioxide (K_C) (not shown here). We tried to find the limit value in which a change in trend in K_C values occurs (growth starts to decrease), in relation to the average wind speed, considering that λ_2 represents the breaking point from which the basic state of the atmospheric system becomes disturbed, generating high variability in all the quantities measured at the surface. This new atmospheric state is characterized by average wind speeds higher than previously works conducted above Amazon forest [24,28]. According to [37], a significant increase in kurtosis of a turbulent quantity (from 2 to 3 times) provides a significant measure of the turbulence's intermittency. In addition, it can be particularly useful for "successfully distinguishing different types of turbulence" [37].

In our dataset, we found a significant change in K_C values for horizontal wind speed above 4.6 m s^{-1}, and from this point on, $\lambda_2 = 4.6$ m s^{-1} is used to identify the beginning of the "very strong" turbulence regime.

For the analysis of the turbulent fluxes of sensible heat ($H = \rho c_p \overline{w'T'}$) and momentum ($\tau = \rho \overline{w'u'}$) associated with each regime, the covariance technique was used for each 5-min of data.

The equivalent potential temperature (θ_E) was calculated according to the thermodynamic equations used by [27] for the tropical atmospheric boundary layer.

$$\theta_E = \theta * exp \left(2675 * \frac{q_v}{T_{LCL}} \right) \tag{5}$$

where θ is the potential temperature, q_V is the mixing ratio of water vapor and T_{LCL} is the temperature at the lifted condensation level [27,38,39].

The value of θ_E was calculated by aggregating contributions of quantities such as pressure and humidity [38] (Chapter 11) [40] (Chapter 4). It provides important information about the convective adjustment of the atmosphere in these high humidity environments [41].

2.2.3. Recurrence Plots for the Analysis of Turbulent Time Series

Recurrence plots are three-dimensional graphs, in which the time series to be analyzed is plotted on the x and y axes and the third dimension are the colors that vary between darker/colder tones (which represents high recurrence) and lighter/hotter tones (low recurrence). If recurring points intensify near an effective transition between two qualitatively distinct states (such as different turbulent regimes), changes in texture patterns are expected to identify this imminent transition. According to [20], the recurrence is a particularly useful method to analyze intervals of time in which the system "repeats certain phases of its trajectory".

For the construction of recurrence graphs, it is necessary to define some important parameters, such as the limit distance (ϵ) between two points in different trajectories, so that they are considered to be recurring, and the time delay (τ) used in the construction of the phase diagram, in its turn providing valuable information about the trajectory of the dynamic system over time [42]. The representation of each point x_i (at time i) in relation to all other points x_j (at time j) of the phase space is given mathematically by:

$$R(i,j) = \Theta(\epsilon - \| x_i - x_j \|) \tag{6}$$

where $i, j = 1 \ldots N - \tau(M - 1)$, $\Theta(x)$ is Heaviside function and the ϵ is a threshold distance, $\| . \|$ is the norm and M is embedding dimension, determined by the false nearest neighbor algorithm [43].

The Heaviside step function delimits values between zero and one. The value zero indicates non-recurring and is represented by lighter/hotter tones and the value one refers to the maximum possible recurrence and is marked with darker/colder tones. The values associated with intermediate

colors are incorporated as a point approaches or distances from that point in relation to which it is desired to estimate the recurrence. According to [42] the Heaviside function Θ is defined by: .

$$\Theta(x) = \{1 \mid x > 0; \ 0 \mid x \leq 0\} \tag{7}$$

The value zero indicates non-recurring and is represented by lighter/hotter tones and the value one refers to the maximum possible recurrence and is marked with darker/colder tones. The values associated with intermediate colors are incorporated as a point approaches or distances from that point in relation to which it is desired to estimate the recurrence.

Here, were applied the methods presented in detail in [20], using the software provided by [43,44]. For the construction of the recurrence diagrams, the time lag $\tau = 8\ s$ and the threshold $\epsilon = 0.1$ for wind speed and temperature and $\epsilon = 0.6$ for the O_3 mixing ratio were used. This "ϵ" threshold was carefully chosen to be not too small to exclude recurring points and not too large to include points of doubtful recurrence [20].

2.2.4. Early-Warning Signals

Many dynamical systems have transition points between different equilibrium states. Locating and understanding these transition points is particularly important to assist in the interpretation of phenomena that occur in nature, such as those that occur in the tropical atmosphere. One of the possibilities to analyze these transition points is using tools such as early-warning signals (EWS) [6,33,45,46]. These tools can be used for emphasizing changes in the properties of statistical categories such as an increase in the values of the autocorrelation function and variance. In this work, we used as a starting point the "early-warning signals toolbox" for detecting critical transitions in time series, provided by [33], whose main characteristics are:

1. One state variable must be selected. To verify which variable best suits as indicator, several tests were performed with the available variables (horizontal and vertical wind velocity, atmospheric pressure, O_3 mixing ratio and θ_E, among others).
2. The autocorrelation at first lag (ACF1) was determined. According to [47] (p. 331), the autocorrelation function, ρ, is defined by:

$$\left[\frac{z(t_1)z(t_2)}{z^2} \right] = \rho(t_2 - t_1) \tag{8}$$

where $z(t)$ is a stationary function at time t, which depends only on the difference $(t_2 - t_1)$ between the two instants t_2 and t_1 in which $z(t_1)$ and $z(t_2)$ values have been measured.
3. The variance of signal was calculated. Mathematically, the unbiased estimator of variance can be given by:

$$\sigma^2 = \frac{1}{n-1} \sum_{t=1}^{n} (z_t - \mu)^2 \tag{9}$$

where μ is the mean value, z_t is the value of the t elements and n is the data number of elements. The autocorrelation function and variance were calculated on a moving window with the length of 10% of the data series. The increment between successive moving windows was one point (1 s).

The objective is to verify whether before the occurrence of an EP a gradual increase of both the autocorrelation function and the variance of the turbulent quantities occurs. Gradual and simultaneous increases of the variance and the autocorrelation function of a state variable are precursors of a transition emergence between two physically distinct states [33,45,46].

To determine the robustness of the estimated trends (increase or decrease) associated with the autocorrelation function and the variance, the coefficient of Kendall [tau] was used. The Kendall [tau] indicator, as proposed by [48], considers a numerical sequence of "n" points which, in our case, is the

number of points used in the autocorrelation function or in variance data series. Each numerical value in this series should be compared to all other subsequent values in the series, in order to form matching and discordant pairs.

The coefficient of Kendall [tau] varies between the limits of −1 to +1, being negative for a sequence of discordant pairs (decreasing trend) and positive for a sequence of matching pairs in which both members of an observation are larger than the pairs of the preceding observation (positive value). The value of Kendall tau is given by the ratio of the resulting score value among the n points of the data series in the form:

$$\tau = \frac{score}{maximum\ possible\ score} = \frac{c - d}{c + d} \tag{10}$$

where c is the number of concordant pairs and d is the number of discordant pairs [48].

We emphasize that the use of wavelet analysis and EWS had the same objective, i.e., to identify the presence of EP. Both methods were used so that there was no doubt regarding the occurrence of these phenomena in our time series. The use of recurrence plot allowed us to precisely locate the emergence of EP. Finally, the phase space of the turbulent regimes were used to show that during the occurrence of an EP there is a transition from a strong turbulent regime to another very strong turbulent regime.

In summary, the following steps were followed in this study, in order to confirm situations of EP occurrence in the tropical NBL:

1. All data were submitted to the quality tests proposed by [49] to verify spurious data in the available time series.
2. Nights with strong variations and sudden changes in turbulent signals of air temperature (>2 K), wind speed (>4.6 m s^{-1}) and increases in O_3-mixing ratio (>10 ppbv) were identified.
3. Selection of nights where there was a transition between the strong to very strong turbulence regimes (λ_2).
4. Selection of an appropriate state variable: a procedure consisting of tests to verify which of the available variables present the best results when submitted to the EWS tests (variables showing positive values for Kendall tau). For our study, three variables were used: wind speed, equivalent potential temperature and O_3-mixing ratio.
5. Definition of the breaking point: the place where the EP starts, using recurrence diagrams (changes in texture patterns are expected to identify this imminent transition), and phase diagrams using Morlet wavelet coefficients (emergence of a phase singularity along the scales from 8192 s to 256 s).

3. Results and Discussion

3.1. Strong Variations in the Turbulent Time Series and Early-Warning Signals

Figure 2 shows that around 0330 UTC (13 April 2014) the horizontal wind velocity increases five-fold (Figure 2a), vertical wind velocity abruptly increases (Figure 2b), θ_E values falls 4 K (Figure 2c), abrupt change in the variance of the barometric surface pressure (Figure 2d), O_3-mixing ratio increases by 10 ppvb (Figure 2e), and sudden increase in air density (Figure 2f). The blue and red lines in Figure 2a,c,e correspond to the autocorrelation function and variance values, respectively, at a moving window calculated for one-point (1 s) increments. Simultaneous increases occur in both autocorrelation and variance function values for all state variables in which the conditions required for critical transition are met (fall in θ_E, and sudden increases in horizontal wind speed and O_3-mixing ratio). The other four nights also investigated in this work are presented in the supplementary material.

Several studies have shown similar simultaneous variations in the presence of deep convection [3,4,26,27]. These strong variations in the time series can be detected by a series of other techniques that will be shown below.
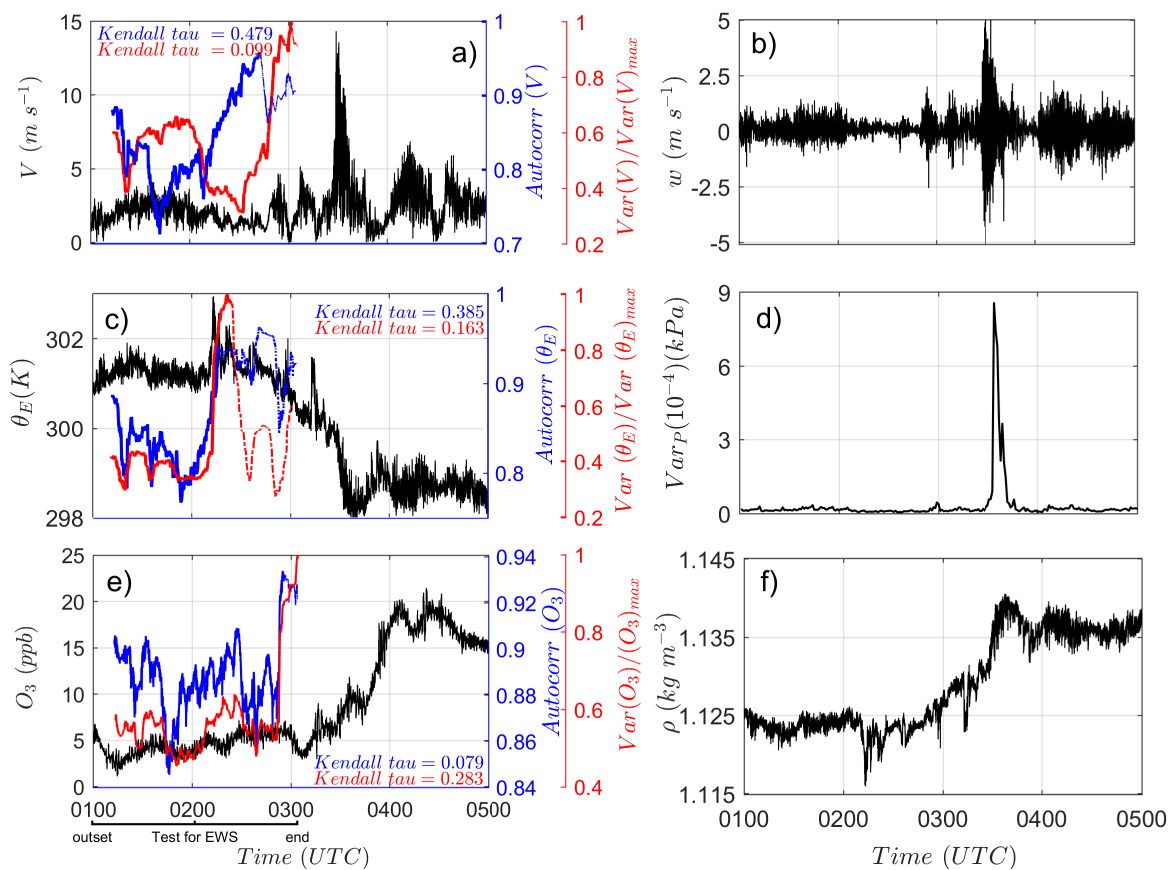
Figure 2. Turbulent time series of: (**a**) horizontal wind velocity (V), (**b**) vertical wind velocity (w), (**c**) equivalent potential temperature (θ_E), (**d**) Pressure variance of the air (Var_P), (**e**) ozone mixing ratio (O_3), and (**f**) air density (ρ). The blue and red lines are the autocorrelation function and variance, respectively. These time series were recorded on 13 April 2014. At 0330 UTC there is an occurrence of extreme phenomena.

It is observed that the trends associated with the autocorrelation function and the variance are in accordance with what is expected for detection of early warnings before abrupt changes (such as the occurrence of EP) in several kinds of temporal processes [33,50], since they tend to grow as an EP approaches. The positive values of Kendall [tau] coefficients qualify the robustness of the indicators along the time series of the state variable [33,50].

The strong variations observed in the thermodynamics time series and O_3-mixing ratio near the surface (Figure 2) and the increase in the autocorrelation function and variance values (Figure 2a,c,e) were associated with occurrence of an EP and whose origin is possibly related to the action of deep convective clouds upon the area of the experimental site. Figure 3 shows the cloud cover in the UTC time corresponding (approximately) to the occurrence of an EP for two (13 April and 16 May 2014) of the five days in which the phenomenon was observed. The radar images for other three days (not shown here) also show an extensive cloud cover above the Cuieiras reserve, during the EP occurrence.

The phenomenon studied here involves the action of convective clouds [27,51]. According to [27], "the fall of θ_E and rise of O_3-mixing ratio are tightly coupled but exactly out of phase, as bursts of downdraft air reach the surface, indicating that the same vertical transport process is responsible for both changes". Also, we observed the occurrence of sudden variations in the pressure signals that became more evident at 35 m height (Figure 2d) (a trend already described by [29] for another set of meteorological data), a few moments before the outbreak of an EP. Such variations in pressure signals

could be associated with downdrafts and updrafts acting over the experimental site, as mentioned by [52] in their study on aerosols evolution cycles above the Amazon forest.
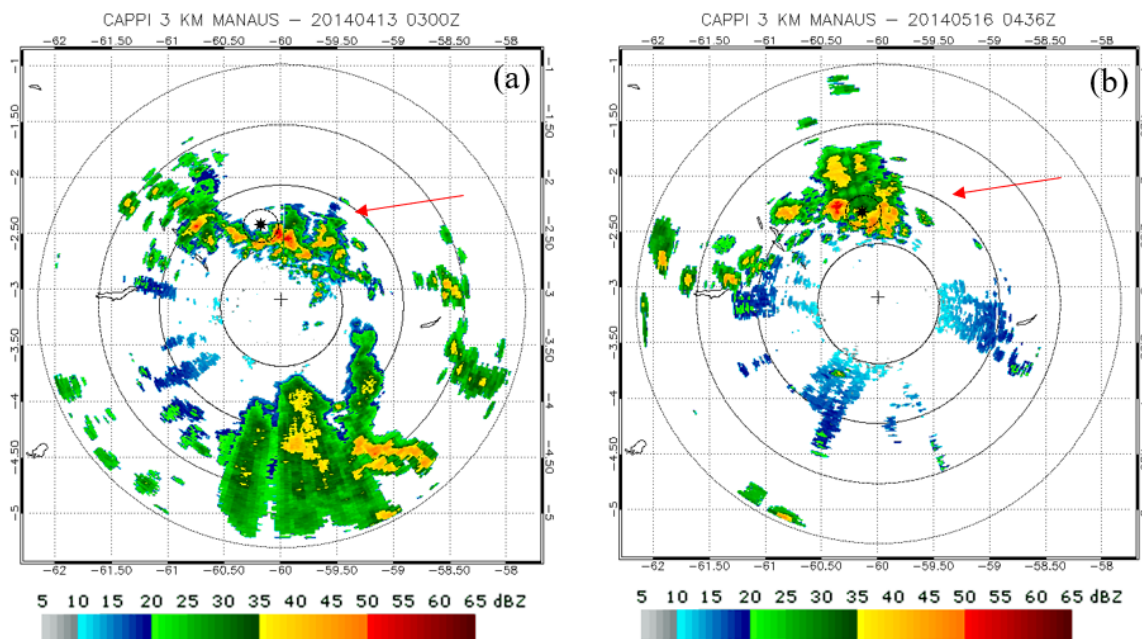

Figure 3. Radar images showing the pattern of cloud cover around the experimental site in periods during occurrences of EP in (**a**) 13 April 2014 at 03 UTC and (**b**) 16 May 2014 at 0436 UTC. The red arrow indicates the direction of the cloud motion and the black point corresponds to the approximate location of the meteorological tower K34. The color bar indicate the corrected equivalent reflectivity factor (dBz). Source: https://iop.archive.arm.gov/arm-iop/2014/mao/goamazon/T1/schumacher-sband_radar/.

3.2. Wavelet and Recurrence Plot Analyses

Morlet wavelet analysis was used to construct a phase space similar to that performed by [17]. Figure 4 shows the time series of horizontal wind speed (*V*) (Figure 4a) and θ_E (Figure 4b) measured at 48 m on 13 April 2014; and time-frequency diagram of the phases of Morlet wavelet coefficients of *V* (Figure 4c) and θ_E (Figure 4d). Figure 4c shows the existence of a main phase singularity along the D_3 axis, which encompasses a range of time scales, from the highest scale (8192 s $\approx$ 2.27 h) to the lowest verified scale (256 s $\approx$ 4.27 min). Also it is possible to verify that there is a drop in temperature that occurs simultaneously with the maximum wind speed (Figure 4b, close to 0330 UTC, indicated by the arrow D_3) and a strong interaction among several physical scales (Figure 4d), with a brief detectable bifurcation below the 512 s scale ($\approx$8.53 min). It is possible to notice the emergence of a phase singularity in a range of various scales, what was discussed by [17] in their analyzed cases of convective processes in the Indonesian atmosphere. They are expressions of non-linear dynamics that can be found in tropical atmospheric dynamics.

Figure 5 presents three recurrence graphs corresponding to the three turbulent variables (*V*, θ_E and O_3 mixing ratio, respectively) selected for this study. The time interval used for the recurrence analyzes was from 01 to 05 UTC. A change of dynamics in the data series can be observed around 0330 UTC for all three turbulent variables used. A sudden change in the dynamics of the system can be observed around 0330 UTC, in which there is an intensification of hotter bands in the recurrence graph for the three turbulent variables used. After this time (around 0330 UTC) the structure resembling a chess board that individualize recurrence processes are no longer verified. These changes in texture patterns provide indications of the occurrence of a transition between two qualitatively distinct states.
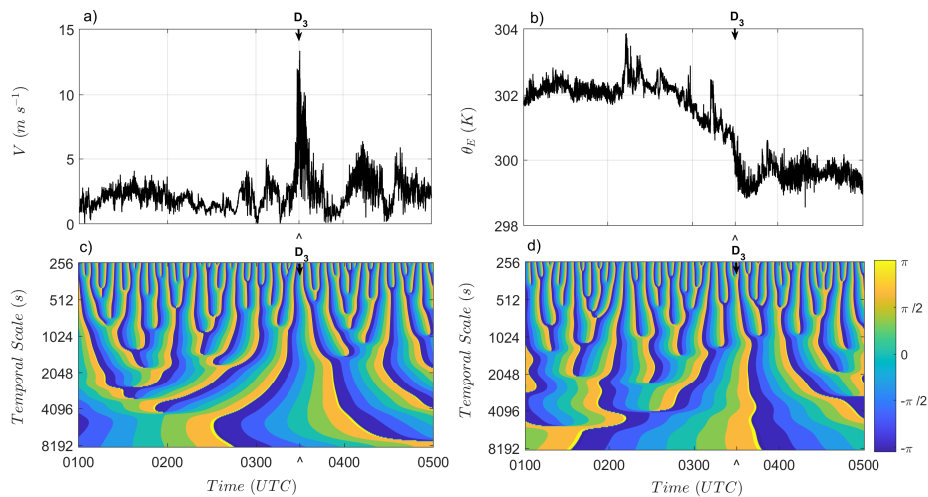
Figure 4. Time series measured at 48 m in 13 April 2014: (**a**) Horizontal wind speed (V); (**b**) equivalent potential temperature (θ_E). Phase of the Morlet wavelet: (**c**) of V and (**d**) θ_E. The arrows D_3 indicate the main phase singularity (during EP).

(**a**)

(**b**)

(**c**)
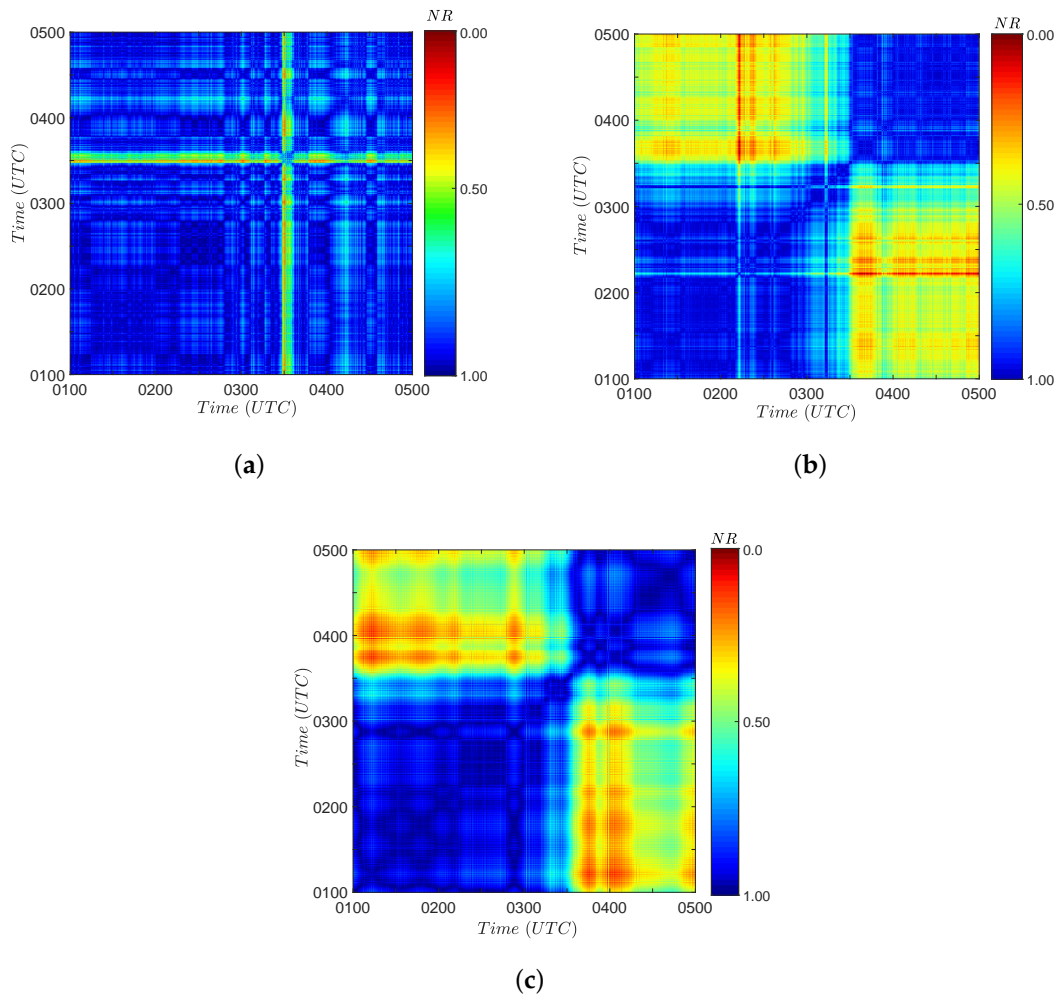
Figure 5. Recurrence plots (RP) for turbulent time series during 13 April 2014: (**a**) horizontal wind speed V (m s^{-1}), (**b**) equivalent potential temperature θ_E (K) and (**c**) O$_3$-mixing ratio (ppb). The vertical bars represent the Recurrence in the form $NR = RP/(RP)_{max}$ corresponding to each one of the three variables.

It is important to note the structures in colder colors (preceding the EP) that can identify the recurrence process [19,20,42] are suppressed after 0330 UTC. Also, at the same time (0330 UTC) there is the existence of a phase singularity (Figure 4c,d). Therefore, it can be assumed that a tipping point (for this particular case) occurred around 0330 UTC.
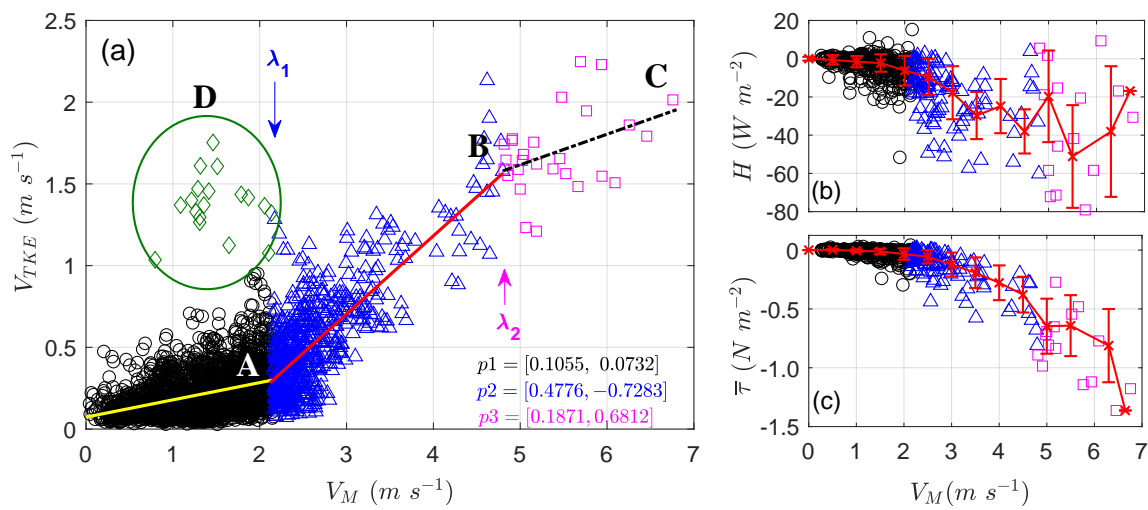
3.3. Turbulence Regimes

To better explain some interesting features of distinct turbulent regimes observed in the NBL, Figure 6a shows the intensity of the turbulence (V_{TKE}) as a function of V_M. For the construction of Figure 6, data from all 5 investigated nights were used, each point corresponding to averages of 5 min. It is possible to notice the presence of several turbulence regimes, which are clustered in 4 regions: around 3 distinct fitted segments (0A, AB and BC) and within the area delimited by the ellipse D, which are present in the Figure 6a. The black circles represent occurrences of the regime of weak turbulence (regime 1, as defined by [25]); the green diamonds represent occurrences of a top-down type of turbulent regime (regime 3, as defined by [25]); the blue triangles and the magenta squares represent occurrences of two kinds of strong turbulence regime (regime 2) that occur in the absence or presence of extreme phenomena (EP's), respectively. Here, the strong turbulence regime (regime 2, as defined by [25]) was split into two sub-sets with different slopes, the first one representing a type of strong turbulence regime (wind speed greater than $\lambda_1 = 2.2$ m s^{-1} and less than $\lambda_2 = 4.6$ m s^{-1}), not associated with EP, and the magenta squares marking the points of strong turbulence regime in which the value of V_M was greater than $\lambda_2 = 4.6$ m s^{-1} and corresponding to situations in which the wind speed was maximum for the analyzed nights. These points ("magenta" squares) were associated with the occurrence of an EP and whose origin is possibly related to the action of deep convective clouds near the experimental site. The occurrence of a very strong turbulence regime, by itself, seems not enough for the generation of an EP. However, it seems that all EP's such as those studied here could be classified as belonging to very strong turbulent regime.

Figure 6b shows the behavior of the flux H over each one of the turbulence regimes presented in the Figure 6a. It is possible to verify that the more intense turbulence regimes are also responsible for the higher intensities of the sensible heat fluxes, which reach -80 W m^{-2} in the very strong turbulence regime. In Figure 6c, the intensity of the vertical flux of u-momentum follows a growing trend for the three turbulence regimes identified in Figure 6a. The red lines shown in Figure 6b,c correspond to the average values of H-turbulent fluxes and momentum flux obtained at each 0.5 m s^{-1} interval for the wind speed and their respective standard deviations. However, for the very strong turbulence regime, an interval of 0.8 m s^{-1} was used due to less data. It is noted that this increasing tendency in momentum flux is not very evident during the weak turbulence regime (black circles), but it becomes clear with the occurrence of the strong turbulence regime (blue triangles), following the same trend during the occurrence of the "very strong" turbulence regime, up to the 7.0 m s^{-1} observed upper limit of V_M velocity.

These results corroborate those presented by [24] for data from Rebio Jarú reserve in South-Western Amazon in which the authors found that there are approximately 40-fold increases in the turbulent sensible heat fluxes during the occurrence of strong turbulence regimes, as compared to weak turbulence regimes. Here, however, it is possible to verify that this increase in H values reaches its maximum value after the second transition (λ_2), i.e., between the strong turbulence regime and a "very strong" turbulence regime.

After the transition from the strong to the very strong turbulence regime, there is a reduction in the intensity of H values with higher mean horizontal wind speeds. This tendency of reduction in the fluxes was also observed by [28]. These authors were able to obtain subsidies that could have led them to the proposition of the existence of a second type of regime of strong turbulence above the Amazon forest. They found a maximum horizontal wind speed of 3.5 m s^{-1} for nighttime data measured at 39.4 and 46.0 m (in the Uatumã reserve, northeast of Manaus, where the Amazon Tall Tower Observatory is located—ATTO). They also used V_{TKE} proposed by [25] to study the variability of CO_2 mixing ratio

and suggested the existence of two different patterns of CO_2 there. But they did not associate their results with the occurrence of EP's above the experimental site.

Figure 6. (**a**) Time evolution of the $V_{TKE} \times V_M$ relationship for the five nights analyzed: λ_1 indicates the transition threshold between the weak turbulence regime and the strong turbulence regime and λ_2 indicates the threshold between the strong and very strong turbulence regimes. The black circles represent occurrences of the weak turbulence regime in 0A segment; the green diamonds inside D ellipse represent occurrences of a top-down type of turbulent regime; the blue triangles in AB segment and the magenta squares near BC segment represent occurrences of two kinds of regime 2 features with strong turbulence regimes split into two sub-sets: the blue triangles, approximately bounded by of the line in red color (above λ_1), represent a type of strong turbulence regime that arises through a "natural" transition, not associated with the occurrence of an EP. The magenta squares mark the points of strong turbulence regime in which the value of V_M was greater than λ_2 and correspond to situations in which the wind speed was maximum for the analyzed nights. p1, p2 and p3 are the slope and offset (i.e., angular and linear) coefficients of the lines 0A, AB and BC, respectively. (**b**) Sensible heat flux and (**c**) kinematic flux of u-momentum over each one of the turbulence regimes presented in the Figure (**a**).

It should be noted that for the case of momentum flux shown in Figure 6c, its intensity does not decrease beyond the λ_2 values, showing only a small reduction in its growth rate immediately after $V_M \approx 4.6$ m s^{-1}. Possibly, the higher increase trend is because vertical and horizontal velocity components continue to grow until the climax of the EP occurrence, thus raising the value of momentum flux. In the case of H, the gradual increase of the wind velocity, associated with the variations in the other turbulent quantities, acts at first to increase the intensity of the fluxes; however, after a certain threshold (λ_2), the wind speed starts to act to reduce the average value of the fluxes instead of increasing it, as was also verified by [28].

Therefore, it is observed that extreme phenomena are atmospheric processes that drive transitional changes in the turbulent regimes and where several phenomena are synchronized, such as: (i) a clear separation between two regions, one of them with smaller air density (before the occurrence of EP) and the other with greater air density (during the occurrence of EP) (Figure 2f) a region where there is a phase lines convergence ("singularities", in the terminology proposed by [17] (Figure 4); (ii) In this region the state variables (in this case, the equivalent potential temperature) validate the criteria formulated in the methodology of [50] (Figure 2c). These transitional changes observed in measurements made at 48 m above the surface, are also noted at other heights, located both above and inside the forest canopy (not shown here), with dramatic shifts in their values during the moment of occurrence of the EP.

4. Conclusions

In this work, experimental data measured in the nocturnal boundary layer, above the Amazon rainforest, were used to analyze strong variations that occur simultaneously in time series (wind speed, temperature, ozone, air humidity, among others). These variations were called extreme phenomena as they significantly affect the turbulent motion in the local boundary layer. The outbreak of these phenomena occurred during the presence of strongly convective clouds, with their respective downdrafts and, consequently, producing strong and well-located increases in pressure variance and air density. Also, it has been shown that these extreme phenomena can be detected by different techniques. One of them analyzed early-warning signals, where there was an increase in the autocorrelation function and in the variance of the state variables immediately before the onset of an extreme phenomena. Morlet wavelet transform is also an efficient tool to identify the beginning of extreme phenomena, since there occurs an intense phase singularity at different frequencies. Also, the recurrence plot technique shows a strong change in atmospheric dynamics, i.e., a transition between qualitatively different atmospheric states. Such a transition is generally expected during the outbreak of an extreme phenomena. Finally, during the occurrence of the extreme phenomena a new category of turbulence regime emerges, classified here as "very strong", where the turbulent fluxes of heat and moment undergo changes completely different from those observed in the absence of the extreme phenomena. All these results demonstrate that during the outbreak of the extreme phenomena, there is a synchronization of events that converge to the same condition of variability.

References

1. Fitzjarrald, D.R.; Moore, K.E. Mechanisms of nocturnal exchange between the rain forest and the atmosphere. *J. Geophys. Res. Atmos.* **1990**, *95*, 16839–16850. [CrossRef]

2. Nogueira, D.S.; Sá L.D.A.; Cohen, J.C.P. Rajadas noturnas e trocas de CO_2 acima da floresta de Caxiuanã, PA, durante a estação seca. *Rev. Bras. Meteorol.* **2006**, *21*, 213–223.

3. Dias-Júnior, C.Q.; Dias, N.L.; Fuentes, J.D.; Chamecki, M. Convective storms and non-classical low-level jets during high ozone level episodes in the Amazon region: An ARM/GOAMAZON case study. *Atmos. Environ.* **2017**, *155*, 199–209. [CrossRef]

4. Melo, A.M.Q.; Dias-Júnior, C.Q.; Cohen, J.C.P.; Sá, L.D.A.; Cattanio, J.H.; Kuhn, P.A.F. Ozone transport and thermodynamics during the passage of squall line in Central Amazon. *Atmos. Environ.* **2019**, *206*, 132–143. [CrossRef]

5. Oliveira, M.I.; Acevedo, O.C.; Sörgel, M.; Nascimento, E.L.; Manzi, A.O.; Oliveira, P.E.S.; Brondani, D.V.; Tsokankunku, A.; Andreae, M.O. Planetary boundary layer evolution over the Amazon rainforest in episodes of deep moist convection at the Amazon Tall Tower Observatory. *Atmos. Chem. Phys.* **2020**, *20*, 15–27. [CrossRef]

6.　Sornette, D. Predictability of catastrophic events: Material rupture, earthquakes, turbulence, financial crashes, and human birth. *Proc. Natl. Acad. Sci. USA* **2002**, *99*, 2522–2529. [CrossRef] [PubMed]

7.　Wu, C.M.; Stevens, B.; Arakawa, A. What controls the transition from shallow to deep convection? *J. Atmos. Sci.* **2009**, *66*, 1793–1806. [CrossRef]

8.　Ghil, M.; Yiou, P.; Hallegatte, S.; Malamud, B.D.; Naveau, P.; Soloviev, A.; Friederichs, P.; Keilis-Borok, V.; Kondrashov, D.; Kossobokov, V.; et al. Extreme events: Dynamics, statistics and prediction. *Nonlinear Proc. Geoph.* **2011**, *18*, 295–350. [CrossRef]

9.　Siebert, J.; Thompson, J.M.T. Nonlinear softening as a predictive precursor to climate tipping. *Philos. Trans. R. Soc. Lond. A* **2012**, *370*, 1205–1227. [CrossRef]

10.　Ashwin, P.; Wieczorek, S.; Vitolo, R.; Cox, P. Tipping points in open systems: Bifurcation, noise-induced and rate-dependent examples in the climate system. *Philos. Trans. R. Soc. Lond. A* **2012**, *370*, 1166–1184. [CrossRef]

11.　Birkhoff, G.; Rota, G.C. *Ordinary Differential Equations*; Wiley: Hoboken, NJ, USA, 1978; p. 342.

12.　Thompson, J.M.T.; Stewart, H.B. *Nonlinear Dynamics and Chaos: Geometric Methods for Engineers and Scientists*; JWS: San Diego, CA, USA, 1986; Volume 1, p. 460f.

13.　Goldstein, J. Emergence as a construct: History and issues. *Emergence* **1999**, *1*, 49–72. [CrossRef]

14.　Lenton, T.M.; Held, H.; Kriegler, E.; Hall, J.W.; Lucht, W.; Rahmstorf, S.; Schellnhuber, H.J. Tipping elements in the Earth's climate system. *Proc. Natl. Acad. Sci. USA* **2008**, *105*, 1786–1793. [CrossRef] [PubMed]

15.　Lenton, T.M. Early warning of climate tipping points. *Nat. Clim. Chang.* **2011**, *1*, 201–209. [CrossRef]

16.　Muller, C.J.; Romps, D.M. Acceleration of tropical cyclogenesis by self-aggregation feedbacks. *Proc. Natl. Acad. Sci. USA* **2018**, *115*, 2930–2935. [CrossRef] [PubMed]

17.　Weng, H.; Lau, K.M. Wavelets, period doubling, and time–frequency localization with application to organization of convection over the tropical western Pacific. *J. Atmos. Sci.* **1994**, *51*, 2523–2541. [CrossRef]

18.　Lau, K.M.; Weng, H. Climate signal detection using wavelet transform: How to make a time series sing. *Bull. Am. Meteorol. Soc.* **1995**, *76*, 2391–2402. [CrossRef]

19.　Trulla, L.L.; Giuliani, A.; Zbilut, J.P.; Webber, C.L., Jr. Recurrence quantification analysis of the logistic equation with transients. *Phys. Lett. A* **1996**, *223*, 255–260. [CrossRef]

20.　Marwan, N.; Romano, M.C.; Thiel, M.; Kurths, J. Recurrence plots for the analysis of complex systems. *Phys. Rep.* **2007**, *438*, 237–329. [CrossRef]

21.　Farias, F.O.M. *Detecção de Fenômenos Extremos na Camada Limite Atmosférica Noturna Acima da Floresta Amazônica a Partir da Análise de Sinais Precursores*; INPA: Manaus, Brazil, 2017; Volume 1, p. 233f.

22.　Martins, H.S.; Sá, L.D.A.; Moraes, O.L.L. Low level jets in the Pantanal wetland nocturnal boundary layer—Case studies. *Am. J. Environ. Eng.* **2013**, *3*, 32–47. [CrossRef]

23.　Sun, J.; Mahrt, L.; Nappo, C.; Lenschow, D.H. Wind and temperature oscillations generated by wave–turbulence interactions in the stably stratified boundary layer. *J. Atmos. Sci.* **2015**, *72*, 1484–1503. [CrossRef]

24.　Dias-Júnior, C.Q.; Sá, L.D.A.; Marques Filho, E.P.; Santana, R.A.; Mauder, M.; Manzi, A.O. Turbulence regimes in the stable boundary layer above and within the Amazon forest. *Agric. For. Meteorol.* **2017**, *233*, 122–132. [CrossRef]

25.　Sun, J.; Mahrt, L.; Banta, R.M.; Pichugina, Y.L. Turbulence regimes and turbulence intermittency in the stable boundary layer during CASES-99. *J. Atmos. Sci.* **2012**, *69*, 338–351. [CrossRef]

26.　Gerken, T.; Wei, D.; Chase, R.J.; Fuentes, J.D.; Schumacher, C.; Machado, L.A.T.; Andreoli, R.V.; Chamecki, M.; de Souza RAFerreira Freire, L.S. Downward transport of ozone rich air and implications for atmospheric chemistry in the Amazon rainforest. *Atmos. Environ.* **2016**, *124*, 64–76. [CrossRef]

27.　Betts, A.K.; Gatti, L.V.; Cordova, A.M.; Dias Maria AFSilva Fuentes, J.D. Transport of ozone to the surface by convective downdrafts at night. *J. Geophys. Res.* **2002**, *107*, LBA 13-1–LBA 13-6. [CrossRef]

28.　Mafra, A.C.B.; de Araújo, A.C.; Sá, L.D.A.; dos Santos, R.M.N.; Trebs, I.; Sorgel, M. Variability of the mean concentration of CO_2 above the amazonian forest during nighttime associated with distinct turbulence regimes. *Ciência Nat.* **2016**, *38*, 429–433.

29.　Acevedo, O.C.; Mahrt, L.; Puhales, F.S.; Costa, F.D.; Medeiros, L.E.; Degrazia, G.A. Contrasting structures between the decoupled and coupled states of the stable boundary layer. *Q. J. R. Meteorol. Soc.* **2015**, *142*, 693–702. [CrossRef]

30. van Hooijdonk, I.G.S.; Moene, A.F.; Scheffer, M.; Clercx, H.J.H.; Van de Wiel, B.J.H. Early warning signals for regime transition in the stable boundary layer: A model study. *Bound. Layer Meteorol.* **2017**, *162*, 283–306. [CrossRef]

31. Kaiser, A.; Faranda, D.; Krumscheid, S.; Belušić, D.; Vercauteren, N. Detecting regime transitions of the nocturnal and Polar boundary layer. *arXiv* **2019**, arXiv:1911.06533.

32. Fuentes, J.D.; Chamecki, M.; Nascimento dos Santos, R.M.; Von Randow, C.; Stoy, P.C.; Katul, G.; Fitzjarrald, D.; Manzi, A.O.; Gerken, T.; Trowbridge, A. Linking meteorology, turbulence, and air chemistry in the Amazon rain forest. *Bull. Am. Meteorol. Soc.* **2016**, *97*, 2329–2342. [CrossRef]

33. Dakos, V.; Carpenter, S.R.; Brock, W.A.; Ellison, A.M.; Guttal, V.; Ives, A.R.; Kefi, S.; Livina, V.; Seekell, D.A.; van Nes, E.H. Methods for detecting early warnings of critical transitions in time series illustrated using simulated ecological data. *PLoS ONE* **2012**, *7*, e41010. [CrossRef]

34. Daubechies, I. Ten lectures on wavelets. *Siam* **1992**, *61*, 1–357f.

35. Farge, M. Wavelet transforms and their applications to turbulence. *Annu. Rev. Fluid Mech.* **1992**, *24*, 395–458 [CrossRef]

36. Sun, J.; Lenschow, D.H.; Burns, S.P.; Banta, R.M.; Newsom, R.K.; Coulter, R.; Frasier, S.; Ince, T.; Nappo, C.; Balsley, B.B. Atmospheric disturbances that generate intermittent turbulence in nocturnal boundary layers. *Bound.-Layer Meteor.* **2004**, *110*, 255–279. [CrossRef]

37. Mahrt, L. Intermittency of atmospheric turbulence. *J. Atmos. Sci.* **1989**, *46*, 79–95. [CrossRef]

38. Holton, J.R. *An Introduction to Dynamic Meteorology*; Elsevier Academic Press: Amsterdam, The Netherlands, 1973; Volume 88, pp. 1–535f.

39. Costantino, L.; Heinrich, P. Tropical deep convection and density current signature in surface pressure: Comparison between WRF model simulations and infrasound measurements. *Atmos. Chem. Phys.* **2014**, *14*, 3113–3132. [CrossRef]

40. Stull, R. *Meteorology for Scientists and Engineers*; UBC: Vancouver, BC, Canada, 2015; pp. 1–295f.

41. Emanuel, K.A. An air-sea interaction theory for tropical cyclones. Part I: Steady-state maintenance. *J. Atmos. Sci.* **1986**, *43*, 585–605. [CrossRef]

42. Marwan, N. Current Developments of Concepts Cased on Recurrence Plots and Their Applications. Ph.D. Thesis, University of Potsdam, Potsdam, Germany, 2003; pp. 1–331f.

43. Chen, Y.; Yang, H. Multiscale recurrence analysis of long-term nonlinear and nonstationary time series. *Chaos Solition Fract.* **2012**, *45*, 978–987. [CrossRef]

44. Yang, H. Multiscale recurrence quantification analysis of spatial cardiac vectorcardiogram signals. *IEEE Trans. Biomed. Eng.* **2011**, *58*, 339–347. [CrossRef]

45. Dakos, V.; Carpenter, S.R.; van Nes, E.H.; Scheffer. M. Resilience indicators: Prospects and limitations for early warnings of regime shifts. *Philos. Trans. R. Soc. B* **2015**, *370*, 20130263. [CrossRef]

46. Lenton, T.M.; Livina, V.N.; Dakos, V.; Van Nes, E.H.; Scheffer, M. Early warning of climate tipping points from critical slowing down: Comparing methods to improve robustness. *Philos. Trans. R. Soc. A* **2012**, *370*, 1185–1204. [CrossRef]

47. Wyngaard, J.C. *Turbulence in the Atmosphere*; Cambridge University Press: Cambridge, UK, 2010; 393p.

48. Kendall, M.G. A new measure of rank correlation. *Biometrika* **1938**, *30*, 81–93. [CrossRef]

49. Vickers, D.; Mahrt, L. Quality control and flux sampling problems for tower and aircraft data. *J. Atmos. Ocean. Technol.* **1997**, *14*, 512–526. [CrossRef]

50. Dakos, V.; Scheffer, M.; van Nes, E.H.; Brovkin, V.; Petoukhov, V.; Held, H. Slowing down as an early warning signal for abrupt climate change. *Proc. Natl. Acad. Sci. USA* **2008**, *105*, 14308–14312. [CrossRef] [PubMed]

51. Wakimoto, R.M. The life cycle of thunderstorm gust fronts as viewed with Doppler radar and rawinsonde data. *Mon. Weather Rev.* **1982**, *110*, 1060–1082. [CrossRef]

52. Wang, J.; Krejci, R.; Giangrande, S.; Kuang, C.; Barbosa, H.M.J.; Brito, J.; Carbone, S.; Chi, X.; Comstock, J.; Ditas, F. Amazon boundary layer aerosol concentration sustained by vertical transport during rainfall. *Nature* **2016**, *539*, 416–419. [CrossRef]